Atmospheric
Chemistry
and Physics
Discussions

Open Access

Enhanced extinction of visible radiation due to hydrated aerosols in mist and fog

T. Elias[1], J.-C. Dupont[2], E. Hammer[4,*], C. R. Hoyle[4,5], M. Haeffelin[2], F. Burnet[3], and D. Jolivet[1]

[1]HYGEOS, Euratechnologies, 59000 Lille, France
[2]Institut Pierre Simon Laplace, 91128 Palaiseau, France
[3]Centre National de Recherche Météorologique, Toulouse, France
[4]Laboratory of Atmospheric Chemistry, Paul Scherrer Institut, 5232 Villigen-PSI, Switzerland
[5]Swiss Federal Institute for Forest Snow and Landscape Research (WSL)-Institute for Snow and Avalanche Research (SLF), 7270 Davos, Switzerland
[*]now at: Grolimund + Partner Ltd – environmental Engineering, Thunstrasse 101A, 3006 Bern, Switzerland

Correspondence to: T. Elias (te@hygeos.com)

ACPD

15, 291–337, 2015

Enhanced extinction of visible radiation due to hydrated aerosols in mist and fog

T. Elias et al.

Title Page

Abstract	Introduction
Conclusions	References
Tables	Figures

|◀ | ▶|
◀ | ▶

Back | Close

Full Screen / Esc

Printer-friendly Version

Interactive Discussion

Abstract

The study assesses the contribution of aerosols to the extinction of visible radiation in the mist-fog-mist cycle. Measurements of the microphysical and optical properties of hydrated aerosols with diameters larger than 400 nm, composing the accumulation mode, which are the most efficient to interact with visible radiation, were carried out near Paris, during November 2011, in ambient conditions. Eleven mist-fog-mist cycles were observed, with cumulated fog duration of 95 h, and cumulated mist-fog-mist duration of 240 h.

In mist, aerosols grew up by taking up water at relative humidities larger than 93 %, causing a visibility decrease below 5 km. While visibility decreased down to few km, the mean size of the hydrated aerosols increased, and their number concentration (N_{ha}) increased from approximately 160 to approximately 600 cm^{-3}. When fog formed, droplets became the strongest contributors to visible radiation extinction, and liquid water content (LWC) increased beyond 7 mg m^{-3}. Hydrated aerosols of the accumulation mode co-existed with droplets, as interstitial non-activated aerosols. Their size continued to increase, and a significant proportion of aerosols achieved diameters larger than 2.5 µm. The mean transition diameter between the accumulation mode and the small droplet mode was 4.0 ± 1.1 µm. Moreover N_{ha} increased on average by 60 % after fog formation. Consequently the mean aerosol contribution to extinction in fog was 20 ± 15 % for diameter smaller than 2.5 µm and 6 ± 7 % beyond. The standard deviation is large because of the large variability of N_{ha} in fog, which could be smaller than in mist or three times larger.

The particle extinction coefficient in fog can be computed as the sum of a droplet component and an aerosol component, which can be approximated by 3.5 N_{ha} (N_{ha} in cm^{-3} and particle extinction coefficient in Mm^{-1}). We observed an influence of the main formation process on N_{ha}, but not on the contribution to fog extinction by aerosols. Indeed in fogs formed by stratus lowering (STL), the mean N_{ha} was 360 ± 140 cm^{-3}, close to the value observed in mist, while in fogs formed by nocturnal radiative cooling

under cloud-free sky (RAD), the mean N_{ha} was $600 \pm 350\,cm^{-3}$. But because visibility (extinction) in fog was also lower (larger) in RAD than in STL fogs, the contribution by aerosols to extinction depended little on the fog formation process. Similarly, the proportion of hydrated aerosols over all aerosols (dry and hydrated) did not depend on the fog formation process.

Measurements show that visibility in RAD fogs was smaller than in STL fogs because: (1) LWC was larger in RAD than in STL fogs, (2) droplets were smaller, (3) as already said, hydrated aerosols composing the accumulation mode were more numerous.

1 Introduction

Aerosols and droplets are major factors of the Earth's radiative budget, as clouds increase the Earth's albedo (Boucher et al., 2013), while aerosol particles may partly counteract global warming by greenhouse gases (Anderson et al., 2003). Moreover fog is responsible for a critical decrease of atmospheric visibility at surface level, with important consequences on transportation activities (Rosenfeld, 1996).

Aerosol particles and fog droplets are responsible for the reduction of visibility by scattering and absorbing light, according to their number and properties, such as size, shape, and chemical composition. Atmospheric humidity is a major factor affecting the particle properties, as aerosols can grow by uptaking water (e.g. Winkler, 1988), when relative humidity increases. Consequently, under conditions of relative humidity larger than 95 %, the aerosol radiative forcing can increase by 60 % (Adams et al., 1999), and atmospheric visibility can be critically reduced (Chen et al., 2012). At relative humidity larger than 100 %, water condensates on some aerosols which are activated, and forms fog droplets (e.g. Jiusto, 1981). This sudden increase in particle size causes a sharp drop in visibility, usually to distances below 1 km. In addition to these droplets, fog also contains interstitial non-activated aerosols, which have a critical supersaturation

Enhanced extinction of visible radiation due to hydrated aerosols in mist and fog

T. Elias et al.

Title Page

Abstract	Introduction
Conclusions	References
Tables	Figures

|◄ | ►|

◄ | ►

Back | Close

Full Screen / Esc

Printer-friendly Version

Interactive Discussion

(Köhler et al., 1937) larger than the peak supersaturation (Hammer et al., 2014a), grow to their stable equilibrium size by taking up water, but do not activate to form droplets.

Numerical weather predictions of fog formation, development and dissipation usually neglect the various aerosol radiative effects, which are:

5   1. decrease of the solar radiation reaching the surface, with potential consequences on late afternoon cooling before fog formation, and on a fog dissipation delay in the morning;

  2. impact on the radiative cooling in the nocturnal boundary layer (Mukund et al., 2014);

10   3. influence on the droplet optical properties, by acting as cloud condensation nuclei (CCN).

Moreover visibility is usually parameterised based on droplet properties uniquely (e.g. Gultepe et al., 2006; Stolaki et al., 2014). However, Jiusto (1981) suggested that a significant amount of the total extinction in fog is due to hydrated aerosol particles of the
15 accumulation mode (with diameters smaller than 2 to 4 µm), which were shown by El-dridge (1966) to be predominant in number. It was shown by Elias et al. (2009) that such aerosols could contribute up to 25 % of the extinction of visible radiation in a fog formed under urban influence.

The current work addresses the contribution of this hydrated aerosol to extinction,
20 and its variability. In the framework of the PreViBOSS project, observation of micro-physical properties of droplets and aerosols was performed during three 6 month fog seasons at SIRTA (Site Instrumental de Recherche par Télédétection de l'Atmosphère, which is French for Instrumented Site for Atmospheric Remote Sensing Research) (Ha-effelin et al., 2005). SIRTA is a platform where other measurements are routinely made,
25 for atmospheric vertical profiling, and sounding of dynamic, thermodynamic and radia-tive properties. We processed the SIRTA database to make connections between (1) aerosol properties and (2) fog properties (visibility and droplet number concentration),

Enhanced extinction of visible radiation due to hydrated aerosols in mist and fog

T. Elias et al.

and atmospheric processes, as those responsible for fog formation: nocturnal radiative cooling or stratus lowering.

Two particle counters measured the microphysical properties of particles in mist and fog, during one month, in ambient conditions, while visibility varied by a factor of 50.
5   Independent measurements of visibility gave the opportunity to validate both mist and fog size distributions, based on Mie theory. Air samples were deliberately not heated, in order to observe the influence of relative humidity on contributing particles to extinction, without hypotheses on aerosol hygroscopicity. Moreover direct measurements were made of both fog droplet and interstitial non-activated aerosol properties, with no need
10 of an inlet system to separate both, and no need of hypotheses regarding the limiting diameter between aerosols and droplets.

Data and methods are presented in Sect. 2. Independent measurements of particle microphysical and optical properties were performed (Sect. 2.1). Mie theory was applied to compute the particle extinction coefficient, inversely proportional to visibil-
15 ity, from measured size distributions, and observed size distributions in fog were approximated by multimodal log-normal distributions, allowing to discriminate between aerosols and droplets and allowing to estimate the impact of hydrated aerosols beyond the diameter of 2.5 µm. The methodology is presented in Sect. 2.2. It is important to distinguish fog and mist, where droplet contribution to extinction is negligible. The iden-
20 tification of mist and fog was based on observed liquid water content, mainly affected by droplets (Sect. 3). Results are presented in Sect. 4. First, a closure study was performed to validate the methodology and to check the data set consistency (Sect. 4.1). Observations are analysed to estimate the mean contribution of hydrated aerosols to extinction of radiation in fog (Sect. 4.2), and their microphysical and optical properties
25 (Sect. 4.3), that we related to the fog formation type (Sect. 4.4). Conclusions are given in Sect. 5.

2   Data and methods

2.1   Measurements

We analysed data acquired in November 2011, when the instrument set-up was optimal. Moreover, November is the most favourable month for mist and fog formation at SIRTA, due to high humidity conditions: around 80 % of observed relative humidity (RH) was larger than 90 %, only 4 % of RH was smaller than 70 %, and the monthly average was 92 ± 9 %. Particle microphysical and optical properties measurements were scheduled by the PreViBOSS project[1] in order to study the impact of aerosols on the fog formation and dissipation, and in particular their impact on radiative transfer in the atmosphere. They were performed during three successive fog seasons from October 2010 to March 2013, coinciding with the ParisFog field campaigns. ParisFog is a series of field campaigns hosted by the SIRTA Observatory and dedicated to describe physical processes in the fog life cycle under contrasted influence of urban pollution and continental/oceanic air masses. SIRTA is located in a suburban area 25 km South West of Paris, covering less than one squared kilometre on the Plateau of Ecole Polytechnique (Haeffelin et al., 2005). The first ParisFog field campaign occurred during the autumn–winter season 2006–2007 (Bergot et al., 2008; Haeffelin et al., 2010). All measurements were made in a continuous mode and at high time frequency (Table 1), to avoid missing any events of reduced visibility. Data were uniformly averaged over 15 min. All times are given in Universal Time (UT).

2.1.1   Aerosol and droplet instrumentation

Particle size distributions were measured in ambient conditions by two optical particle counters (Table 1). The WhitE Light Aerosol Spectrometer-2000 (WELAS; PALAS Gmbh, Karlsruhe, Germany) and the Fog Monitor-100 (FM100; Droplet Measurement Technologies, Boulder, CO, USA) together provided size distributions of aerosols and

[1]http://hygeos.com/fr/previboss.htm

Title Page

Abstract | Introduction

Conclusions | References

Tables | Figures

|◄ | ►|

◄ | ►

Back | Close

Full Screen / Esc

Printer-friendly Version

Interactive Discussion

droplets with diameters between 400 nm and 50 µm in ambient conditions. In the WE-LAS optical chamber, the air sample is illuminated by a white light and the scattered radiation is measured at a scattering angle of 90° angle (Heim et al., 2008). In the FM100, the forward-scattered light of a 0.658 µm laser beam is measured in the 4–12° angular range. It is expected that the particle counter efficiency is reduced close to the size detection limits. Thus, the systematic number concentration gradient recorded by WELAS in the 400–800 nm diameter size range might be an instrument artefact (Fig. 1). Consequently, the minimum size detection is 400 nm when commenting the hydrated aerosol number concentration, but the minimum size detection is 800 nm when dealing with the hydrated aerosol size distribution, then the 11 first bins, over 66 bins, are disregarded. The WELAS size output was calibrated in laboratory by sounding latex particles with prescribed size, while the number concentration output was not calibrated. A "reference" instrument was then dedicated to intercalibrate both WELAS and FM100 in field conditions: a co-located DF20+ diffusometer (Degreane Horizon) provided independent measurements of both visibility and particle (aerosol and fog droplet) extinction coefficient. According to the manufacturer, the uncertainty is ±10 % below a visibility of 5 km, and ±15 % between 5 and 20 km (uncertainties presented in Table 1). Uncertainty of less than ±10 % is not achievable with diffusometer sensors (Crosby, 2003).

The volume size distribution provided by FM100 was integrated over size to provide the liquid water content (LWC, in $mg\,m^{-3}$) (e.g. Wendisch, 1998). A Particle Volume Monitor-100 (PVM; Gerber Scientific, Inc., Reston, Virginia, USA) was also running, exploited here to confirm or complement LWC values given by the FM100 (Burnet et al., 2012). A TSI CPC instrument mounted behind a $PM_{2.5}$ inlet also measured aerosol number concentration for dry diameter between 4 nm and 2.5 µm. All aerosol and droplet instruments were set up 4 m a.g.l.

2.1.2 Meteorological data

Thermohygrometric profiles, cloud base height and precipitation were parameters used to describe the atmospheric conditions prevalent at mist and fog formation and dissipa-

tion. Vertical profiles of temperature and RH were acquired by a 30 m meteorological mast. A Vaisala CL31 ceilometer detected the cloud presence above the site and also estimated the cloud base height, at 1 min resolution. Precipitation was measured by standard gauge devices and sedimentation was observed by a YES TPS310 instru-
5 ment.

2.2 Methodology

Here, we describe the methodology to compute the particle extinction coefficient for several particle populations, which were defined according to the measured size distributions. The aerosol contribution to extinction of visible radiation in fog can then be
10 estimated (Sect. 4). Computations were compared to the particle extinction coefficient independently observed by the diffusometer, for validation in two steps: computations for aerosols alone in mist; computations for aerosols and droplets in fog (Sect. 4.1). The distinction between mist and fog is presented in Sect. 3.

2.2.1 Computation of the particle extinction coefficient

15 The particle extinction coefficient, which is usually expressed in Mm^{-1} ($10^{-6} m^{-1}$), was derived by two independent methods. The particle extinction coefficient (pec_K) was first directly provided by the DF20+, according to the Koschmieder equation (e.g. Hess et al., 1998):

$$pec_K = \frac{-\ln(C_V)}{\text{visibility}} \times 10^6 \qquad (1)$$

20 Visibility (in m) is a measure of the distance where contrast between an object and its background can be viewed by the unaided eye. With a visual contrast C_v of 5 %, fixed by the manufacturer, usual thresholds of 1 and 5 km in visibility correspond to pec_K of around 3000 and 600 Mm^{-1}, respectively. A wavelength of 550 nm is representative of the lamp spectrum.

The particle extinction coefficient (pec_M) was also derived by the Mie theory applicable to spherical aerosol particles (e.g. Bohren and Huffman, 1983):

$$pec_M = \sum_{D_{min}}^{D_{max}} \frac{\pi D^2}{4} \, \Delta N(D) \, Q_{ext}(D, \lambda = 550\,nm, m) \tag{2}$$

The Mie extinction efficiency factor Q_{ext} (D, λ, m) depends on the radiation wavelength λ, the particle diameter D (in µm), and the refractive index m, which is assumed to be independent of wavelength and time. The AEROsol Robotic NETwork (Holben et al., 1998) provided indicative values of the refractive index of ambient aerosols present in the whole atmospheric column over the SIRTA, on 13, 19, 20 and 22 November 2011. The imaginary part varied between 0.04 and 0.10, indicating presence of absorbing particles typical of urban and industrialized pollution (Shettle and Fenn, 1979), and the real part varied between 1.40 and 1.55. $m = 1.45 - 0.05i$ was used for hydrated interstitial aerosol particles of diameter smaller than 2.5 µm and the refractive index of pure water, $m = 1.33 - 0i$, was used for particles larger than 2.5 µm in diameter, which are mainly composed of water (Table 2). $\Delta N(D)$ is the particle size distribution (in cm^{-3}). pec_M is directly proportional to the number concentration N (in cm^{-3}), as:

$$pec_M = N \frac{\pi}{4} \sum_{D_{min}}^{D_{max}} D^2 f(D) Q_{ext}(D, \lambda = 550\,nm, m) \tag{3}$$

with

$$N = \sum_{D_{min}}^{D_{max}} \Delta N(D) \tag{4}$$

and

$$\Delta N(D) = N f(D) \tag{5}$$

30 % uncertainty was estimated on pec_M, taking into account the instrumental errors, the uncertainties from the two systems to provide the particle size distribution $\Delta N(D)$, the hypotheses on the refractive index, and the assumptions used in the optical property algorithm.

5 For validating the methodology and the data set, comparisons were made between pec_K and pec_M (see results in Sect. 4.1). In mist, the size distribution of aerosols alone (Sect. 2.2.2) was used in Eq. (2) and in fog, the size distribution of both aerosols and droplets was used. Burnet et al. (2012) showed some comparisons of size distributions acquired by WELAS and FM100. The FM100 values were far lower than

10 the WELAS values for particles smaller than 5 µm in diameter, whereas the WELAS values were lower than the FM100 values for particles larger than 10 µm in diameter. The FM100 has indeed the purpose to complement the WELAS in regards to larger particles. Among the two instruments, the instrument giving largest values is assumed to provide the most reliable measurements, thanks to its greatest sensitivity. Conse-

15 quently, the junction diameter of 7 µm was chosen for processing all data. The WELAS then provided the size distribution of interstitial hydrated aerosols and droplets smaller than 7 µm (Elias et al., 2009), while the FM100 provided the size distribution of droplets larger than 7 µm.

2.2.2 Definition of hydrated aerosols

20 Fog is composed of droplets and interstitial non-activated aerosols. As noted by Whitby (1978) and others, the particle size distribution can be expressed by superimposed lognormal distributions. From the WELAS measurements, it can be seen that some of the interstitial aerosols compose the accumulation mode. It is commonly accepted that the lower bound of this mode is 0.1 µm, but the upper bound varies between 1 and

25 2.5 µm according to several authors (Noone et al., 1992; Seinfeld and Pandis, 1998). Moreover diameters in dry conditions are usually given, when they can further increase in humid conditions. As the WELAS size distribution is not reliable below the diameter of 800 nm, the WELAS is not the best choice to measure aerosols with sizes near

the lower bound of the accumulation mode, but it is definitely adapted for the upper bound. As long as the mode maximum can be identified by the WELAS, as well as the upper bound, and that most of the mode size range is sounded, we assumed that WELAS could provide the three parameters defining the accumulation mode: number concentration, mode diameter and width. Examples shown in Fig. 1 illustrate the large variability of the size distributions, concerning all 6 parameters: size, width, number modes.

This approach allowed us to let the hydrated aerosol size interval varying in fog, with no need to arbitrarily fix an aerosol size limit, as was the 2.5 μm threshold of Elias et al. (2009). The droplet mode provided by WELAS was also approximated by a log-normal distribution and we then inferred the diameter transition between aerosols and droplets in fog, measured in ambient conditions. The diameter transition was defined as the intersection between the two approximated modes of the volume size distributions. It was between 3 and 5 μm in the examples of Fig. 1. For the computations with Mie theory (Eq. 2), we fixed D_{min} and D_{max} values as reported in Table 2. In fog, Eq. (2) then becomes:

$$pec_M = \Delta_{ha}pec_M + \Delta_d pec_M \tag{6a}$$

or,

$$pec_M = \Delta_{ha,D<2.5\,\mu m}pec_M + \Delta_{ha,D>2.5\,\mu m}pec_M + \Delta_d pec_M \tag{6b}$$

with $\Delta_d pec_M$ the droplet contribution, and $\Delta_{ha}pec_M$ the aerosol contribution, which can be divided according to the aerosol diameter smaller or larger than 2.5 μm.

3 Fog and mist definitions

In this study, fog is identified with criteria other than the 1 km convention, as presented in the chart flow of Fig. 2. A detailed explanation and justification of the use of these

criteria follows in this section. The 1 km convention could not be applied because of the necessity to discriminate events regarding the droplet presence, for both the closure study and the computation of the aerosol contribution to extinction.

3.1 Fog

According to the National Oceanic and Atmospheric Administration (1995), fog is a collection of suspended water droplets near the Earth's surface that lead to a reduction of horizontal visibility below 1 km. Aerosols are activated, and droplets form when RH increases beyond a threshold that is usually between 100 and 101 %, depending on various factors (Hammer et al., 2014b). The uncertainty is too high to use RH to detect aerosol activation. Consequently other thresholds are used to detect fog presence. As a matter of fact, as droplet formation has important consequences on visibility, fog is conventionally defined according to thresholds on visibility prescribed by transport considerations, which vary between 400 m (e.g. Meyer and Lala, 1990) and 5 km (e.g. Jiusto, 1981). Jiusto (1981) presented a discussion about the visibility threshold. Elias et al. (2009) proposed a further criterion on temporal gradient of visibility, and Berkowitz et al. (2011) on accumulated precipitation.

However both aerosols and droplets affect visibility (e.g. Elias et al., 2009) and visibility may even be reduced below 1 km without droplets but by aerosols (Quan et al., 2011). The event is then called smog (Pearce, 1992) or unactivated fog (Frank et al., 1998). Meanwhile, formation of droplets also has important consequences for LWC which is a direct indicator of the condensation process. For example LWC changes by a factor larger than visibility during fog formation (Heintzenberg et al., 1998). In this context, we chose to set a threshold based on LWC values.

Fog is defined according two criteria: on 15 min averages of LWC, and on the time change of LWC over three 15 min time steps. First, fog occurs if LWC $> 7\,\mathrm{mg\,m^{-3}}$. Figure 3 shows that LWC ranged from 7 to $20\,\mathrm{mg\,m^{-3}}$ at visibility of 1 km. The lowest bound is then chosen as the threshold for defining fog. This is close to $10\,\mathrm{mg\,m^{-3}}$ used by Wendisch et al. (1998) as a threshold to consider measurements of LWC. This is

consistent with smallest values of 8 or 9 mg m^{-3} for coastal fogs (Jiusto, 1981), and of 20 mg m^{-3} observed by Wobrock et al. (1992).

Moreover, we consider fog presence if LWC < 7 mg m^{-3}, with however visibility < 1 km and LWC > 7 mg m^{-3} during the previous and the next time step (Fig. 2). Figure 3 shows that this situation occurred rarely, only 5 times, which is less than 2 % of the fog situations and less than 0.05 % of the cases with visibility < 5 km. Moreover we suspect that FM100 did not provide appropriate values of LWC in such cases, as the PVM, in contrary to FM100, showed values of LWC larger than 10 mg m^{-3}.

Heintzenberg et al. (1998) set a threshold of 2 mg m^{-3} for defining fog. This is the minimum possible value for a threshold as aerosols alone can contribute up to few mg m^{-3}: haze could contribute to 1.4 mg m^{-3} (Eldridge, 1966), or aerosols to 0.45 mg m^{-3} at 95 % RH (Pandis and Seinfeld, 1990). Moreover 7 mg m^{-3} seems appropriate for long-lasting fogs as according to Eldridge (1966), LWC values below 6 mg m^{-3} were found only in evolving fog, which is a transition between fog and mist.

Moreover, according to observations reported by Elias et al. (2012), we checked the fog spatial homogeneity, with a temperature vertical gradient from the surface up to 30 m height smaller than 0.04 °C m^{-1} (Elias et al., 2012).

Fog visibility was observed between 1 and 3 km (Fig. 3), on 14 occasions, when fog usually formed or dissipated. Consistently, Meyer et al. (1980) observed that droplets were formed at 1–2 km visibility range, and Jiusto (1981) defined light fog by visibility between 1 and 5 km. Such visibility was caused by few rather large droplets that contributed more to LWC and less to the extinction coefficient: the droplet effective diameter was larger than the monthly average of 15 ± 3 mm (similar to Wendisch et al., 1998), and droplet number concentration was smaller (8–45 cm^{-3}) than the monthly average of 100 ± 50 cm^{-3}. That high values of fog visibility demonstrate that the diffusometer alone is not able to distinguish the main cause of the visibility reduction, between aerosols or droplets. Only twice (on 17 and 26 November), such high values of visibility associated to values of LWC > 7 mg m^{-3} were however disregarded as fog because: (1) such event each lasted less than 30 min, and (2) visibility reached values larger

Title Page

Abstract | Introduction

Conclusions | References

Tables | Figures

◀ | ▶|

◀ | ▶

Back | Close

Full Screen / Esc

Printer-friendly Version

Interactive Discussion

than 5 km before and after this event. Moreover, averaged LWC did not go beyond 11 mg m^{-3}. Such cases were labelled "no-fog mist".

As a result of the described protocol applied to November 2011 SIRTA data, 18 fogs aggregated into 11 mist-fog-mist cycles were observed, for a cumulated mist-fog-mist duration of 240 h, and a cumulated fog duration of 95 h. Fog properties are presented in Table 3.

3.2 Mist

The visibility change during the mist-fog transition was due to the droplet formation, while most visibility changes in mist occurred due to the aerosol growth. While fog is defined by LWC > 7 mg m^{-3}, mist is defined by LWC < 7 mg m^{-3}. Since mist was a low visibility event, we also defined mist by visibility < 5 km. As stated by Clark et al. (2001), visibility is a more precise measurement of the impact of RH than the the the proper measurement of RH. For example, uncertainty of 1 % in RH at RH > 95 % reports as an uncertainty of 20 % in visibility (or extinction coefficient) (Chen at al., 2012), larger than the DF20+ uncertainty.

Rain drops can also decrease visibility, and a further criterion was applied to not merge rain and mist events. Mist is defined by a precipitation rate smaller than 0.4 mm h^{-1} (Fig. 2), which was the detection limit of the instrument. Consistently with Heintzenberg et al. (1998), the impact of the fog formation was stronger on LWC than on visibility: average LWC in mist was found to be approximately a factor larger than 50 lower than that in fog, while the average visibility in mist was a factor of 5 to 11 higher than that in fog (Table 3).

Quan et al. (2011) showed that haze and mist are usually distinguished according to RH. Consistently, mist RH at SIRTA was larger than 93 % and the monthly average was 99 %. At SIRTA, thick haze in dry conditions did not occur in November 2011 and visibility < 5 km was always caused by mist or fog. With such high values of RH, we expect that aerosols responsible for low visibility were hydrated. In this paper we define

"hydrated aerosols" as the aerosols of the accumulation mode which are responsible for visibility reduction in mist, and measured by WELAS.

3.3 The mist-fog-mist cycle and the no-fog mist

Some mist events preceded fog events, others followed the fog events, and some could be intermediate between two fog events. They were named pre-fog, post-fog, and in-fog respectively. Mist-fog-mist cycle was defined as a continuous low visibility event (visibility < 5 km), with water droplets observed for at least 45 min. The chronological sequence is composed basically as mist-fog-mist, but also as mist-fog-mist-fog-mist, etc. Mist always preceded fog, even if in two cases (c10 and c11, Table 3), pre-fog mist was not observed in the 15 min step data set. Pre-fog mist was then observed in the 1 min time resolution, as visibility decreased from 10 km to less than 1 km in 15 min. In two other cases (c1 and c6), mist was not observed before the fog formation, because they started as shallow fog patches, which are disregarded here.

No-fog mist was also a low visibility event (visibility < 5 km), but which never occurred before or after a fog event. Visibility was observed smaller than 5 km during around 45 h of no-fog mist, and during other 145 h of pre-fog, in-fog, or post-fog mist. Clear-air was defined by visibility larger than 10 km.

3.4 Fog formation types

The cloud fraction measured by the CL31 ceilometer was used to distinguish the main fog formation process (e.g. Tardif and Rasmussen, 2007) observed at SIRTA. The cloud fraction is $N_{clouds}/15$, with N_{clouds} the number of minutes (1 min CL31 measurement period) when cloud was observed, in a 15 min time step. Cloud fraction was averaged during the 5–10 km visibility event preceding the mist-fog-mist cycle, and the associated standard deviation was computed. The distribution of the cloud fraction values showed two distinct modes: when the cloud fraction was larger than 70 %, with a standard deviation smaller than 30 %, the fog formed due to stratus lowering (STL); when the

cloud fraction was smaller than 30 %, with a standard deviation smaller than 30 %, the fog formed by radiative cooling (RAD). Threshold values were fixed to classify all cases observed at SIRTA. Six fog life cycles started after radiative cooling and five due to stratus lowering. Our fog identification generally agrees to identify fog events, with the method of Tardif and Rasmussen (2007) applied on November 2011 SIRTA data by Menut et al. (2013) for the radiative fogs, but is more detailed concerning the exact start and end times. The mist-fog-mist cycles $c1$, $c4$, $c5$ and $c10$ correspond to the Fog Observation Periods FOP1, FOP2, FOP3 and FOP9 of Menut et al. (2013). The $c6$ event which started as a shallow fog corresponds to the FOP8 identified as entirely shallow by Menut et al. (2013). The $c2$ event is not listed by Menut et al. (2013) and consistently with our method the 26 November fog is not listed neither, but on contrary the short fog event of 17–18 November is considered (FOP4). Moreover our method provides more insight on the details of the fog interruptions by mist.

Rapid changes of visibility observed before fog formation in the $c10$ and $c11$ cycles could be due to fog advection to SIRTA. Indeed the wind speed increased to more than $2\,\mathrm{m\,s}^{-1}$ at the $c10$ fog onset, and it was even larger during the $c11$ mist-fog-mist cycle. Such conditions favour advective fog formation as described by Tardif and Rasmussen (2007). Low cloud ceiling (cloud base height smaller than 800 m) before the $c11$ fog formation, suggests that the stratus was pushed away while the fog was advected to SIRTA, which seemed similar to the "CBL fog 1" category defined by Van Schalkwyk and Dyson (2013). We added the term ADV to name these two events.

Mist preceding STL fog lasted usually longer than mist preceding RAD fog (Table 3). Indeed pre-fog mists lasted less than one hour in RAD mist-fog-mist cycles, while three pre-fog mists lasted more than 4 h in STL mist-fog-mist cycles. Consequently, we observed only 2 cumulated hours of pre-fog mist for RAD fogs, and more than 12 h of pre-fog mist for STL fogs. As also observed by Tardif and Rasmussen (2007), RAD fogs were on average more opaque than STL fogs, with visibility of 290 ± 210 and 570 ± 430 m, respectively. Larger droplets were observed in STL than in RAD fogs (effective radius of 8.0 ± 1.2 and 6.8 ± 1.4 mm, respectively). Consistently, fog visibility

observed larger than 1200 m occurred only in STL and never in RAD fogs. Moreover larger LWC occurred in RAD than in STL fogs (Table 3). Contrary to Tardif and Rasmussen (2007), the longest fog events were found to result from radiative cooling, such as the $f2$ and $f7$ fogs which lasted more than 10 h each (Table 3).

Low cloud ceiling was systematically observed by the ceilometer over the pre-fog mists: low stratus for the STL fog, and an elevated fog layer forming when visibility at surface level was already smaller than 5 km, after nocturnal radiative cooling. The typical case of the $c4$ mist-fog-mist cycle (15 November 2011) was presented in detail by Stolaki et al. (2014): the fog formed at around 150 m a.g.l., and in 30 min the base reached the surface. Eventually, the average cloud base height was always smaller than 120 m over pre-fog mist. During other months of the ParisFog field campaign, some RAD fogs were also observed to appear at surface level and not as an elevated fog layer. Low cloud cover was also observed above in-fog mist, meaning that the interruption of a fog in a same fog life cycle was due to stratus lifting and lowering.

4 Results

4.1 Validation of the instrument set up and methodology

A closure study was performed, by estimating the particle extinction coefficient with two independent methods and making comparisons (method presented in Sect. 2.2). The efficiency of the WELAS to probe aerosols was examined by making comparisons in mist, and the efficiency of combined WELAS and FM100 to probe both aerosols and droplets was examined by making comparisons in fog. Values of the ratio pec_M/pec_K for different events are given in Table 4.

4.1.1 Aerosols responsible for low visibility in mist

The particle extinction coefficient measured by the DF20+ was reproduced by the WELAS measurements and Mie theory (within combined uncertainties of 40 %) when hy-

Title Page

Abstract | Introduction

Conclusions | References

Tables | Figures

◄ | ►

◄ | ►

Back | Close

Full Screen / Esc

Printer-friendly Version

Interactive Discussion

drated aerosols of the accumulation mode were responsible for the visibility reduction. This was the case in mist preceding fogs (Fig. 4) with an average ratio $\text{pec}_M/\text{pec}_K$ of $86 \pm 22\,\%$, when pec_K varied between 600 and 2200 Mm^{-1}. A fraction of the under-estimation observed below 1000 Mm^{-1} could be due to the under-estimation of the
5   hydrated aerosol number concentration at diameters smaller than 800 nm.

4.1.2   Combined WELAS and FM100 in fog

Agreement between measurements and computations was satisfying in fog (Fig. 5), when WELAS and FM100 measurements were combined, with an average ratio of $107 \pm 35\,\%$. During the $f1$ and $f9$ fogs, FM100 measurements showed a high number
10   of droplets larger than 20 µm which caused LWC to increase above 200 mg m^{-3}, and pec_M to be much larger than pec_K. These values did not agree with measurements made by the PVM, they were consequently screened out from the data set (PVM and FM100 eventually agreed with a slope of 0.80). Moreover, the relation between LWC and visibility shown in Fig. 3 is consistent with observations presented by Heintzenberg
15   et al. (1998). Therefore the WELAS and FM100 combined together were considered appropriate to measure both aerosols and droplets responsible for extinction in fog.

As a conclusion, according to the agreement in the particle extinction coefficient, in both pre-fog mist and fog events, we consider that WELAS provided the aerosol number concentration in ambient conditions in fog with sufficient precision.
20   The measurements also show conditions when the WELAS did not properly count the particles responsible for visibility reduction. The FM100 was observed to miss droplets in shallow fog patches (Elias et al., 2012), which were consequently not considered here. Similarly, the WELAS alone did not reproduce the extinction coefficient in mist preceding shallow fog patches. Moreover, we have noted that even in cloud-free
25   no-fog mist, $\text{pec}_M/\text{pec}_K$ reduced to $53 \pm 23\,\%$ if the temperature vertical gradient was larger than $0.04\,°\text{C m}^{-1}$, and reached $95 \pm 21\,\%$ if it was smaller (Table 4). That shows

that the criterion on the thermal vertical gradient seems discriminative for defining the optimal measurement conditions of the WELAS.

4.1.3   Drops missed by both WELAS and FM100

The mist and fog criteria (Fig. 2) disregard the low visibility events caused by rain. We comment these situations in this section to provide hints on specific cases when the particle counters do not provide satisfaction in regards to aerosols and fog droplets. Visibility was reduced below 5 km by drops during eleven rain events, witnessed by a precipitation rate larger than $0.4\,\mathrm{mm\,h^{-1}}$. As the drop size exceeded both the WELAS and FM100 sensitivity domains, these instruments can not provide the size distribution of all particles responsible for the visibility decrease, and $\mathrm{pec}_M/\mathrm{pec}_K$ was only $25 \pm 12\,\%$ during these events. Similarly, we suspect that large particles undetected by the particle counters were sometimes responsible for the visibility reduction below 5 km, still with a precipitation rate smaller than $0.4\,\mathrm{mm\,h^{-1}}$. These large particles could be caused by drizzle, expected when the cloud ceiling was very low. Indeed, $\mathrm{pec}_M/\mathrm{pec}_K$ was only $43 \pm 20\,\%$ (Table 4) when the cloud base height was smaller than 100 m (according to the CL31 ceilometer) in no-fog mist. However the WELAS observations were validated in no-fog mist below cloud-free sky, as $\mathrm{pec}_M/\mathrm{pec}_K$ was $78 \pm 30\,\%$, with a main mode included between 50 and 120 %, as for pre-fog mist. Moreover the TPS310 instrument confirmed the suspicion of drizzle in three of these low-cloud ceiling no-fog mist events, as it showed a signal of sedimentation at a rate of less than $0.4\,\mathrm{mm\,h^{-1}}$, not detectable by a standard rain sensor.

In post-fog mist conditions, the WELAS instrument was unable to measure all aerosols contributing to extinction, as already observed by Elias et al. (2009) for one case study of February 2007. In November 2011, visibility was similar in pre-fog and post-fog mists, but the hydrated aerosol number concentration was 40 % smaller in post-fog mist. Drizzle may then often occur after the fog dissipations, with drizzle drops beyond the size domain sensitivity of the particle counters.

These observations also indicate that at SIRTA fogs formed in November 2011 after mist composed by hydrated aerosols, and never after rain neither drizzle. Consistently Haeffelin et al. (2013) also observed that liquid water deposition (0.2 mm accumulated precipitation in 3 h) prevented vertical development of a fog layer at SIRTA on 20 February 2007.

4.2 Contribution to fog extinction by hydrated aerosols

Aerosols contributed significantly to the extinction of visible radiation in fog. It is known that visibility in fog is mainly governed by LWC (Fig. 3), but also by the particle size. For constant LWC, visibility decreases with decreasing particle size. Following this principle, aerosols are too small to contribute significantly to LWC but can not be neglected in terms of extinction. The hydrated aerosols smaller than 2.5 μm contributed to the extinction of visible radiation observed in fog up to $\Delta_{\mathrm{ha},D<2.5\,\mu m}\mathrm{pec}_M/\mathrm{pec}_K = 20\pm15\,\%$ (Fig. 6a), and the hydrated aerosols larger than 2.5 μm contributed as $\Delta_{\mathrm{ha},D>2.5\,\mu m}\mathrm{pec}_M/\mathrm{pec}_K = 6\pm7\,\%$ (Fig. 6b). $\Delta_{\mathrm{ha},D<2.5\,\mu m}\mathrm{pec}_M/\mathrm{pec}_K$ partly depended on fog visibility, as it was smaller than 5 % in long lasting fogs where visibility was often smaller than 200 m, as during $f1$, $f2$ and $f16$ fogs, and it was smaller than 20 % when visibility was smaller than 600 m. In contrast, it was between 40 and 70 % when fog visibility was between 300 and 1000 m. Dependence on visibility was not found for $D > 2.5\,\mu m$.

Visibility parameterisations incorporated in numerical modelling of fog usually consider only droplets (e.g. Gultepe et al., 2006; Stolaki et al., 2014). We present the consequences of not considering aerosols. According to Eq. (5a), if $\mathrm{pec}_K = \mathrm{pec}_M$, the droplet extinction coefficient is:

$$\Delta_{\mathrm{d}}\mathrm{pec}_M = \mathrm{pec}_K - \Delta_{\mathrm{ha}}\mathrm{pec}_M, \tag{7a}$$

or

$$\Delta_{\mathrm{d}}\mathrm{pec}_M = \mathrm{pec}_K - \langle\mathrm{aecs}\rangle N_{\mathrm{ha}} \tag{7b}$$

where $\langle aecs \rangle$ is the average aerosol extinction cross section, which represents the efficiency of one particle to extinguish visible radiation. N_{ha} is the hydrated aerosol number concentration. $\langle aecs \rangle$ varied between 2.4 and $4.3 \times 10^{-8} \, cm^2$, depending on the method, the aerosol diameter range and the mist/fog event (Table 5). Indeed, we observed a correlation between pec_K and N_{ha} (Fig. 7) in mist, providing $\langle aecs_{mist} \rangle = 3.0 \times 10^{-8} \, cm^2$. It is interesting to note that such a method does not depend on the size attribution by WELAS. Because of the aerosol size increase in fog, $\langle aecs_{fog} \rangle$ was slightly larger than $\langle aecs_{mist} \rangle$. Dividing $\Delta_{ha}pec_M$ by N_{ha} in fog resulted in $\langle aecs_{fog} \rangle = 3.5 \times 10^{-8} \, cm^2$ for $D < 2.5 \, \mu m$ and in $\langle aecs_{fog} \rangle = 4.3 \times 10^{-8} \, cm^2$ for aerosols both below and beyond $2.5 \, \mu m$.

The impact of not considering aerosols in fog visibility is significant, as visibility of $380 \pm 320 \, m$ was observed, while the value of $530 \pm 490 \, m$ was computed without aerosols (for a constant value of LWC), setting $\langle aecs \rangle = 3.5 \times 10^{-8} \, cm^2$ in Eq. (7b). When only droplets were considered, the number of visibility values around $400 \, m$ was critically reduced, and more values were found between 1 and 2 km. As a consequence, with the 1 km convention to detect fog, a proportion of 17 % of the fog events would be missed by considering only extinction due to droplets, while only 4 % of the fog events would be missed by considering both aerosols and droplets. For example, fog would last only 2.5 h during the $c4$ mist-fog-mist cycle, instead of the six observed cumulated hours, and it would start 30 min later than what was observed according to the LWC threshold (Table 3). Similarly, Ahmed et al. (2014) show that the minimum droplet concentration necessary to reach 1 km visibility is reduced if aerosols are considered, with consecutive impact on fog detection by satellite.

As soon as supersaturation occurred, the visibility drop in some fogs did not occur only due to droplet formation but also due to the increase of N_{ha}. Indeed, at $f7$ and $f9$ fog onsets, the contribution by hydrated aerosols alone was sometimes larger than $3000 \, Mm^{-1}$ (with number concentration larger than $800 \, cm^{-3}$), resulting in a contribution to fog extinction between 30 and 50 %. However, at SIRTA such high aerosol

Enhanced extinction of visible radiation due to hydrated aerosols in mist and fog

T. Elias et al.

Title Page

Abstract | Introduction

Conclusions | References

Tables | Figures

|◄ | ►|

◄ | ►

Back | Close

Full Screen / Esc

Printer-friendly Version

Interactive Discussion

extinction coefficient was never observed outside a fog event. The influences of both N_{ha} and the aerosol size are described in next Section.

4.3 Hydrated aerosol microphysical properties

4.3.1 Hydrated aerosol number concentration

In pre-fog mist, the aerosol growth due to hydration caused both an increase of N_{ha} and the visibility reduction: high RH induced a large aerosol growth factor (Chen et al., 2011), and the number of aerosols growing larger than 400 nm was large enough to be responsible for visibility reduction from 5 to few km. While pec_K increased from 600 to 2200 Mm^{-1} in pre-fog mist (Fig. 7), N_{ha} increased from 160 to 600 cm^{-3}, which was similar to observations presented by Kunkel (1984).

On average, 60 % more hydrated aerosols were observed in fog than in mist, but the standard deviation was larger by a factor of 3. Averages of N_{ha} in fog varied by a factor of five (Table 3), and instantaneous values could vary by a factor of three during the same fog event. For example, during $f9$ fog the number concentration decreased by more than 1000 cm^{-3} in 5 h, while during $f2$ fog it increased by an equivalent magnitude. During $f7$ and $f8$ fogs, a succession of increases and decreases was observed. During these four fogs, the number concentration reached values much larger than those observed in pre-fog mist. However, the number concentration could also be smaller than in pre-fog mist, as was the case during $f1$ and $f16$ fogs, when it decreased down to around 200 cm^{-3} after the fog onset. The rate of change of N_{ha} mostly ranged between −300 and 300 cm^{-3} h^{-1}. The variability of number concentration in individual fog events then increased with fog duration: the standard deviation was smaller than 15 % when fog lasted 1 h, but it was larger than 50 % when fog lasted more than 12 h. In pre-fog mist, the mean rate of change of N_{ha} was 100 cm^{-3} h^{-1}.

In mist, most aerosols larger than 400 nm were hydrated. Figure 8 shows that a number concentration larger than 200 cm^{-3} was observed only in very humid conditions, and the accumulation mode aerosols were on average ten times more numerous in

pre-fog mist than in clear-air (Table 3). With a mean number concentration of aerosols of all size (N_C), according to CPC, of $5200 \pm 2100\,\mathrm{cm}^{-3}$, around $7 \pm 3\,\%$ of aerosols were larger than 400 nm in pre-fog mist.

4.3.2 Hydrated aerosol size

Such variability in the number concentration was not observed in the size parameters. On the contrary, a net tendency of increase of the hydrated aerosol size was observed during both the pre-fog mist and the mist-fog transition. Therefore the aerosol extinction coefficient in fog increased because of the average N_{ha} but also because of the accumulation mode extending to larger sizes.

In pre-fog mist, the accumulation mode diameter increased from 0.8 to more than 1.3 μm and simultaneously the mode width increased from 1.3 to more than 1.5 (Fig. 7b and c) when pec_K increased. This observed tendency explains that the hydrated aerosol size was too small at a visibility of $\sim 5\,\mathrm{km}$ to be properly measured by WELAS (see Sect. 4.1.1).

In fog, the accumulation mode still widened, with a mean mode width increasing from 1.36 ± 0.06 in pre-fog mist to 1.57 ± 0.10 in fog. The mode width was frequently larger than 1.5 in fog but rarely in mist. Moreover the accumulation mode shifted towards larger sizes, with a mean mode diameter increasing from $0.93 \pm 0.11\,\mathrm{\mu m}$ in pre-fog mist to $1.14 \pm 0.15\,\mathrm{\mu m}$ in fog (Fig. 9). The mode diameter was frequently larger than 1.0 μm in fog but rarely in mist. Consequently, a significant proportion of hydrated aerosols was found beyond the diameter of 2.5 μm, while they were rarely found in pre-fog mist. Indeed, the transition diameter transition between aerosols and droplets was $4.0 \pm 1.1\,\mathrm{\mu m}$ (Fig. 9). According to Chen et al. (2011), such large aerosols are made possible by the large hygroscopic growth factor which sharply increases with RH and can be larger than 3 at RH of 99 % for aerosols of dry diameter of 250–1000 nm. Consistently, Stolaki et al. (2014) showed that the number concentration of aerosols included between 200 and 500 nm dry diameter, measured by a TSI SMPS particle counter, was of the same order of magnitude as the hydrated aerosols measured by the WELAS.

A constant value to separate aerosols to droplets, was fixed at e.g. 5 µm by Noone et al. (1992), and at 3 µm by Hoag et al. (1999). However measurements made in ambient conditions by the WELAS instrument showed a significant variability of the diameter transition between aerosols and droplets. The transition diameter varied between 2 and 8 µm, and was more frequently between 3 and 5 µm in November 2011. Similar results were reported by Hammer et al. (2014b). The hydrated aerosols larger than 2.5 µm were not numerous ($35 \pm 30\,\mathrm{cm}^{-3}$, reaching sometimes $100\,\mathrm{cm}^{-3}$), but, as shown in Sect. 3.2, their large size implied a significant contribution to extinction.

Measurements presented by Elias et al. (2009) suggested that the influence of pollution was higher on 18–19 February 2007 than in November 2011: more aerosols (6000–$15\,000\,\mathrm{cm}^{-3}$ in fog), more hydrated aerosols, but smaller with mode diameter of 0.6 µm. Eventually, the 25 % aerosol contribution was similar to here.

4.4 Influence of the fog formation processes

We used observations to explain the high variability of the hydrated aerosol number concentration. First, we used the aerosol number concentration of all sizes measured by CPC (N_C), to study the impact of the potential changes of the boundary layer height. Then, we examined the impact of the main fog formation processes.

In relation to aerosols of all sizes, more hydrated aerosols of the accumulation mode were found in fog than in pre-fog mist, with the fog ratio N_{ha}/N_C of 10 ± 7 %. Variability was large, and significant changes observed during $f1$ and $f2$ fogs were not caused by potential changes in the mixing boundary layer height. Indeed changes in the mixing boundary layer height are expected to affect all sizes of aerosols similarly, which was not the case on these dates. Figure 10a shows that during the $f1$ fog and part of the $f2$ fog, N_{ha} slightly increased when N_C also increased, while during the other part of the $f2$ fog, N_{ha} varied by a factor of three while N_C remained close to $4000\,\mathrm{cm}^{-3}$. However, we observed that there was an influence of the fog formation process on the aerosol number concentration. More hydrated aerosols were found in RAD fogs than in STL fogs, with $600 \pm 350\,\mathrm{cm}^{-3}$ and $360 \pm 140\,\mathrm{cm}^{-3}$, respectively (Table 3). Values of fog

averages of N_{ha} between 200 and 650 cm^{-3} were observed in both STL and RAD fogs, while values larger than 650 cm^{-3} were encountered only in the RAD fogs (Fig. 10a and Table 3). Similarly, more aerosols of all sizes were found in RAD than in STL fogs. Indeed, according to the CPC data, we observed 6400 ± 2600 cm^{-3} aerosols in RAD fogs, and 4000 ± 1400 cm^{-3} aerosols in STL fogs.

Observations showed tendencies between the particle properties which witness the aerosol indirect effect on the radiative budget. First, a large number of aerosols would restrict the droplet growth (e.g. Albrecht, 1989). Consistently, Elias et al. (2012) show that the droplet size decreased when the droplet number concentration increased for RAD and STL fogs of November 2011. This paper presents that a larger number of smaller droplets is correlated with a larger number of aerosols (of all sizes and hydrated), and that occurred in RAD fogs. Moreover LWC was larger in RAD than in STL fogs. Consequently visibility in RAD was smaller than in STL by an average of 280 m, or pec_K was larger by 5000 Mm^{-1}. Aerosols contributed around 20 % to the RAD-STL visibility difference. Indeed, using an aerosol extinction cross section of 4×10^{-8} cm^2, the aerosol extinction coefficient was around 1600 Mm^{-1} in STL and around 2700 Mm^{-1} in RAD. Droplets were therefore responsible for around 4000 Mm^{-1} in the RAD-STL difference. While there is a significant correlation of the fog formation process with N_{ha}, the correlation with the aerosol contribution to extinction was not observed, with 24 ± 16 % in STL and 19 ± 14 % in RAD fogs.

Considering that hydrated aerosols are potential condensation nuclei for the formation of fog droplets (Meyer et al., 1980), a large reservoir of nuclei was usually available. Compared to the accumulation mode number, 23 ± 18 % of droplets were observed in fog. The ratio N_d/N_{ha} could be larger than 40 % when N_{ha} was minimum, as during the RAD $f1$, STL $f16$, and RAD $f17$ fogs. Figure 10b shows that N_{ha} during the $f1$ fog is close to the minimum while N_C is the mid range. However during the $f2$ fog, for similar values of N_C, N_{ha} is larger than 500 cm^{-3} and has a tendency to increase with N_C.

Title Page

Abstract | Introduction

Conclusions | References

Tables | Figures

◄ | ►

◄ | ►

Back | Close

Full Screen / Esc

Printer-friendly Version

Interactive Discussion

5 Conclusions

The purpose of the research was to estimate the contribution of aerosols to the extinction of visible radiation in mist and fog, and its variability. Comparisons between particle extinction coefficients derived by Mie theory and measured independently showed that the instrument set-up was appropriate to fulfil our objectives.

The size distribution of hydrated aerosols in the accumulation mode, responsible for extinction of visible radiation in mist, was measured in ambient conditions. Visibility decreased below 5 km due to an increase in size of some of the aerosols, due to water intake in high relative humidity conditions. The accumulation mode widened (mode width from 1.3 to 1.5) and shifted to larger sizes (mode diameter from 0.8 to 1.3 μm) while visibility decreased down from 5 to few km. The hydrated aerosol number concentration (N_{ha}) increased from 160 to 600 cm^{-3}.

The hydrated aerosols contributed significantly to the extinction of visible radiation in fog. Fog was composed of interstitial non-activated aerosols and of droplets which provided liquid water content (LWC) larger than 7 mg m^{-3}. The hydrated non-activated aerosols continued to grow from mist to fog: the accumulation mode diameter increased to 1.14 ± 0.15 μm, and the mode width increased from 1.36 ± 0.06 in mist to 1.57 ± 0.10 in fog. Moreover N_{ha} increased from 330 ± 100 to 520 ± 320 cm^{-3}, from mist to fog. Consequently the hydrated aerosols smaller than 2.5 μm contributed by an average of 20 % to extinction. The maximum aerosol diameter was found to be variable and often larger than 2.5 μm, with an average of 4.0 ± 1.1 μm. Aerosols larger than 2.5 μm were not numerous (35 ± 30 cm^{-3}) but they contributed by a further 6 ± 7 % to extinction in fog. Visibility lower than 1 km was caused by LWC greater than 7 mg m^{-3}, but could also be caused by N_{ha} larger than 800 cm^{-3}. However, such large hydrated aerosol number concentration at SIRTA was observed only in high humidity conditions which also triggered droplet formation.

The particle extinction coefficient in fog can be computed as the sum of an aerosol and a droplet components. The aerosol component can be approximated by 3.5 N_{ha},

Title Page

Abstract | Introduction

Conclusions | References

Tables | Figures

|◄ | ►|

◄ | ►

Back | Close

Full Screen / Esc

Printer-friendly Version

Interactive Discussion

with 3.5×10^{-8} cm^2 being the aerosol extinction cross section estimated in our study. Consequently, observed fog visibility was 380 ± 320 m but it would be 530 ± 490 m if only droplets were accounted for, with constant LWC (aerosols contributing little to LWC). 4 % of the fog visibility was observed larger than 1 km, but 17 % of the fog visi-
5 bility would be larger than 1 km, if only droplets were considered.

Part of the large variability observed in N_{ha} was related to the fog formation process. Observations showed tendencies consistent with the aerosol indirect effect: more aerosols were observed in radiative cooling fogs (RAD) than in stratus lowering fogs (STL), and droplets were smaller and more numerous in RAD than in STL fogs. More-
10 over LWC was larger in RAD than in STL fogs. Consequently visibility in RAD was lower than in STL by an average of 280 m. However the formation process had little influence on the aerosol contribution to fog extinction. Large variability remains unexplained, for example observed N_{ha} changes were not always correlated with changes of number concentration of aerosols of all size or of droplets.
15 Radiative transfer computations will be performed in the future. We will quantify the contribution of hydrated aerosols on the radiative budget: impact of mist on radiative cooling, impact of the aerosols on solar heating of the surface layer and on the dissipation time. Microphysical properties of aerosols and droplets are required, but also other properties such as their vertical profile which was also sounded at SIRTA and
20 which is currently analysed. To fully describe the relations between fog and aerosols, we should also study aerosols smaller than ~ 800 nm in diameter. No direct measurements were made of such aerosols is ambient conditions, but one method is to convert available TSI SMPS measurements made in the dry state (e.g. Hammer et al., 2014b). new instrumentation may also provide interesting results (Renard et al., 2014).

Enhanced extinction of visible radiation due to hydrated aerosols in mist and fog

T. Elias et al.

Title Page

Abstract	Introduction
Conclusions	References
Tables	Figures

|◄   ►|

|◄   ►|

Back   Close

Full Screen / Esc

Printer-friendly Version

Interactive Discussion

References

Adams, P. J., Seinfeld, J. H., and Koch, D. M.: Global concentration of tropospheric sulfate, nitrate, and ammonium aerosol simulated in a general circulate model, J. Geophys. Res., 104, 13791–13823, 1999.

Ahmed, R., Dey, S., and Mohan, M.: A study to improve night time fog detection in the Indo-Gangetic Basin using satellite data and to investigate the connection to aerosols, Met. Apps., doi:10.1002/met.1468, 2014.

Albrecht, B.: Aerosols, cloud microphysics, and fractional cloudiness, Science, 245, 1227–1230, 1989.

Anderson, T., Charlson, R. J., Schwartz, S. E., Knutti, R., Boucher, O., Rodhe, H., and Heintzenberg, J.: Climate forcing by aerosols: a hazy picture, Science, 300, 1103–1104, 2003.

Bergot, T., Haeffelin, M., Musson-Genon, L., Tardiff, R., Colomb, M., Boitel, C., Bouhours, G., Bourriane, T., Carrer, D., Challet, J., Chazette, P., Drobinski, P., Dupont, E., Dupont, J.-C., Elias, T., Fesquet, C., Garrouste, O., Gomes, L., Guérin, A., Lapouge, F., Lefranc, Y., Legain, D., Morange, P., Pietras, C., Plana-Fattori, A., Protat, A., Rangognio, J., Raut, J.-C., Remy, S., Richard, D., Romand, B., and Zhang, X.: Paris-Fog : des chercheurs dans le brouillard, La Météorologie, 8, 48–58, doi:10.4267/2042/19175, 2008.

Berkowitz, C. M., Berg, L. K., Yu, X. Y., Alexander, M. L., Laskin, A., Zaveri, R. A., Jobson, B. T., Andrews, E., and Ogren, J. A.: The Influence of fog and airmass history on aerosol optical, physical and chemical properties at Pt. Reyes National Seashore, Atmos. Environ., 45, 2259–2568, doi:10.1016/j.atmosenv.2011.02.016, 2011.

Bohren, C. F. and Huffman, D. R.: Absorption and Scattering of Light by Small Particles, John Wiley, New York, 1983.

Boucher, O., Randall, D., Artaxo, P., Bretherton, C., Feingold, G., Forster, P., Kerminen, V.-M., Kondo, Y., Liao, H., Lohmann, U., Rasch, P., Satheesh, S. K., Sherwood, S., Stevens, B., and Zhang, X. Y.: Clouds and aerosols, in: Climate Change 2013: the Physical Science Basis, Contribution of Working Group I to the Fifth Assessment Report of the Intergovernmental Panel on Climate Change, edited by: Stocker, T. F., Qin, D., Plattner, G.-K., Tignor, M., Allen, S. K., Boschung, J., Nauels, A., Xia, Y., Bex, V., and Midgley, P. M., Cambridge University Press, Cambridge, UK and New York, NY, USA, 571–657, 2013.

Burnet, F., Gomes, L., Haeffelin, M., Dupont, J. C., and Elias, T.: Analysis of the Microphysical Structures of Fog During the ParisFog Project, in: Proceedings of the 16th international

Title Page

Abstract | Introduction

Conclusions | References

Tables | Figures

⏮ | ⏭

◀ | ▶

Back | Close

Full Screen / Esc

Printer-friendly Version

Interactive Discussion

conference of clouds and precipitation (ICCP), Leipzig, Germany, 30 July–3 August, 582, 2012.

Chen, J., Zhao, C. S., Ma, N., Liu, P. F., Göbel, T., Hallbauer, E., Deng, Z. Z., Ran, L., Xu, W. Y., Liang, Z., Liu, H. J., Yan, P., Zhou, X. J., and Wiedensohler, A.: A parameterization of low visibilities for hazy days in the North China Plain, Atmos. Chem. Phys., 12, 4935–4950, doi:10.5194/acp-12-4935-2012, 2012.

Clark, P. A. and Hopwood, W. P.: One-dimensional site-specific forecasting of radiation fog, Part I: Model formulation and idealised sensitivity studies, Meteorol. Appl., 8, 279–286, doi:10.1017/S1350482701003036, 2001.

Crosby, J. D.: Visibility sensor accuracy: what's realistic?, in: 12th Symposium on Meteorological Observations and Instrumentation, Long Beach, CA, 15.5, 13 February 2003.

Eldridge, R. G.: Haze and fog distributions, J. Atmos. Sci., 23, 605–613, 1966.

Elias, T., Haeffelin, M., Drobinski, P., Gomes, L., Rangognio, J., Bergot, T., Chazette, P., Raut, J.-C., and Colomb, M.: Particulate contribution to extinction of visible radiation: pollution, haze, and fog, Atmos. Res., 92, 443–454, 2009.

Elias, T., Jolivet, D., Dupont, J.-C., Haeffelin, M., and Burnet, F.: Preliminary results of the Pre-ViBOSS project: description of the fog life cycle by ground-based and satellite observation, in: Proc. SPIE 8534, Remote Sensing of Clouds and the Atmosphere XVII; and Lidar Technologies, Techniques, and Measurements for Atmospheric Remote Sensing VIII, 853406 (1 November 2012), edited by: Kassianov, E. I., Comeron, A., Picard, R. H., Schäfer, K., Singh, U. N., and Pappalardo, G., doi:10.1117/12.974709, 2012.

Frank, G., Martinsson, B. G., Cederfelt, S., Berg, O. H., Swietlick, E., Wendisch, M., Yuskiewicz, B., Heitzenberg, J., Wiedensohler, A., Orsini, D., Stratmann, F., Laj, P., and Ricci, L.: Droplet formation and growth in polluted fogs, Beitr. Atmos. Phys., 71, 65–85, 1998.

Gultepe, I., Müller, M. D., and Boybeyi, Z.: A new visibility parameterization for warm-fog applications in numerical weather prediction models, J. Appl. Meteorol. Clim., 45, 1469–1480, 2006.

Haeffelin, M., Barthès, L., Bock, O., Boitel, C., Bony, S., Bouniol, D., Chepfer, H., Chiriaco, M., Cuesta, J., Delanoë, J., Drobinski, P., Dufresne, J.-L., Flamant, C., Grall, M., Hodzic, A., Hourdin, F., Lapouge, F., Lemaître, Y., Mathieu, A., Morille, Y., Naud, C., Noël, V., O'Hirok, W., Pelon, J., Pietras, C., Protat, A., Romand, B., Scialom, G., and Vautard, R.: SIRTA, a ground-based atmospheric observatory for cloud and aerosol research, Ann. Geophys., 23, 253–275, doi:10.5194/angeo-23-253-2005, 2005.

Enhanced extinction of visible radiation due to hydrated aerosols in mist and fog

T. Elias et al.

Title Page

Abstract	Introduction
Conclusions	References
Tables	Figures

|◄ | ►|

◄ | ►

Back | Close

Full Screen / Esc

Printer-friendly Version

Interactive Discussion

Köhler, H.: The nucleus in and the growth of hygroscopic droplets, T. Faraday Soc., 32, 1152–1161, 1936.

Kunkel, B. A.: Parameterization of droplet terminal velocity and extinction coefficient in fog models, J. Clim. Appl. Meteorol., 23, 34–41, 1984.

Menut, L., Mailler, S., Dupont, J.-C., Haeffelin, M., and Elias, T.: Predictability of the meteorological conditions favorable to radiative fog formation during the 2011 ParisFog campaign, Bound.-Lay. Meteorol., 150, 277–297, doi:10.1007/s10546-013-9875-1, 2013.

Meyer, M. B. and Lala, G. G.: Climatological aspects of radiation fog occurrence at Albany, New York, J. Climate, 3, 577–586, 1990.

Meyer, M. B., Jiutso, J. E., and Lala, G. G.: Measurements of visual range and radiation-fog (haze) microphysics, J. Atmos. Sci., 37, 622–629, 1980.

Mukund, V., Singh, D. K., Ponnulakshmi, V. K., Subramanian, G., and Sreenivas, K. R.: Field and laboratory experiments on aerosol-induced cooling in the nocturnal boundary layer, Q. J. Roy. Meteor. Soc., 140, 151–169, doi:10.1002/qj.2113, 2014.

National Oceanic and Atmospheric Administration: Surface Weather Observations and Reports, Federal Meteorological Handbook, vol. 1, Washington, DC, 94 pp., 1995.

Noone, K. J., Ogren, J. A., Hallberg, A., Heintzenberg, J., Ström, J., Hansson, H. C., Svenningsson, B., Wiedensohler, A., Fuzzi, S., Facchini, M. C., Arends, B. G., and Berner, A.: Changes in aerosol size- and phase distributions due to physical and chemical processes in fog, Tellus B, 44, 489–504, 1992.

Pandis, S. N. and Seinfeld, J. H.: The smog-fog-smog cycle and acid deposition, J. Geophys. Res., 95, 18489–18500, 1990.

Pearce, F.: Back to the days of deadly smogs, New Sci., 1850, 25–28, 1992.

Quan, J., Zhang, Q., He, H., Liu, J., Huang, M., and Jin, H.: Analysis of the formation of fog and haze in North China Plain (NCP), Atmos. Chem. Phys., 11, 8205–8214, doi:10.5194/acp-11-8205-2011, 2011.

Renard, R. J.-B, Dulac, D. F., Berthet, B. G., Lurton, L. T., Vignelles, V. D., Tonnelier, T. T., Thaury, T. C., Jeannot, J. M., Coute, C. B., Akiki, A. R., Mineau, M. J.-L., Verdier, V. N., Mallet, M. M., Gensdarmes, G. F., Charpentier, C. P., Mesmin, M. S., Duverger, D. V., Dupont, D. J.-C., Elias, E. T., Crenn, C. V., Sciare, S. J., Giacomoni, G. J., Gobbi, G. M., Hamonou, H. E., Olafsson, O. H., Dagsson-Waldhauserova, D.-W. P., Camy-Peyret, C.-P. C., Mazel, M. C., Dechamps, D. T., Piringer, P. M., Jegou, J. F., Surcin, S. J., and Daugeron, D. D.: LOAC: a small aerosol optical counter/sizer for ground-based and balloon measurements of the size

distribution and nature of atmospheric particles 1. Principle of measurements and instrument evaluation, Atmos. Meas. Tech., in press, 2014.

Rosenfeld, J.: Cars vs. the weather. A century of progress, Weatherwise, 49, 14–23, 1996.

Seinfeld, J. H. and Pandis, S. N.: Atmospheric Chemistry and Physics: from Air Pollution to Climate Change, John Wiley, New York, 1360 pp., 1998.

Shettle, E. P. and Fenn, R. W.: Models for the Aerosols of the Lower Atmosphere and the Effects of Humidity Variations on their Optical Properties, AFGL-TR-79-0214, Environmental Research Paper Air Force Geophysics Lab., Hanscom AFB, MA. Optical Physics Div., 94 pp., 1979.

Stolaki, S., Haeffelin, M., Lac, C., Dupont, J.-C., Elias, T., and Masson, V., Influence of aerosols on the life cycle of a radiation fog event. A numerical and observational study, Atmos. Res., 151, 146–161„ doi:10.1016/j.atmosres.2014.04.013, 2014.

Tardif, R. and Rasmussen, R. M.: Event-based climatology and typology of fog in the New York City region, J. Appl. Meteorol. Clim., 46, 1141–1168, 2007.

van Schalkwyk, L. and Dyson, L. L.: Climatological characteristics of fog at Cape Town international airport, Weather Forecast., 28, 631–646, doi:10.1175/WAF-D-12-00028.1, 2013.

Wendisch, M.: A quantitative comparison of ground-based FSSP and PVM measurements, J. Atmos. Sci. Tech., 15, 887–900, 1998.

Wendisch, M., Mertes, S., Heintzenberg, J., Wiedensohler, A., Schell, D., Wobrock, W., Frank, G., Martinsson, B. G., Fuzzi, S., Orsi, G., Kos, G., and Berner, A.: Drop size distribution and LWC in Po Valley fog, Beitr. Atmos. Phys., 71, 87–100, 1998.

Whitby, K. T.: The physical characteristics of sulfur aerosols, Atmos. Environ., 12, 135–159, 1978.

Winkler, P.: The growth of atmospheric aerosol particles with relative humidity, Phys. Scr., 37, 223–230, 1988.

Wobrock, W., Schell, D., Maser, R., Kessel, M., Jaeschke, W., Fuzzi, S., Facchini, M. C., Orsi, G., Marzorati, A., Winkler, P., Arends, B. G., and Bendix, J.: Meteorological characteristics of the Po Valley fog, Tellus B, 44, 469–488, 1992.

Enhanced extinction of visible radiation due to hydrated aerosols in mist and fog

T. Elias et al.

Title Page

Abstract	Introduction
Conclusions	References
Tables	Figures

|◄ | ►|

◄ | ►

Back | Close

Full Screen / Esc

Printer-friendly Version

Interactive Discussion

Table 1. Instrumental set-up at SIRTA for the measurement of particle properties in ambient and dry (only CPC) conditions.

Instrument	Observed parameters	Particle diameter range (µm)	Sampling time resolution	Uncertainty
Degreanne DF20+ diffusometer	Visibility (and extinction coefficient)	all	1 min	±10 % (visibility < 5 km)
Vaisala CL31 ceilometer	Cloud fraction and cloud base height	all	30 s	±15 m
PALAS WELAS particle counter	Number size distribution	0.40–42	5 min	Number concentration: ±20 %
DMT FM100 particle counter	Number size distribution (and liquid water content, droplet effective radius)	2–50	1 s	
Gerber PVM	Liquid water content	3–50	1 s	±15 %
TSI CPC	Dry aerosol number concentration	Dry: 0.04–2.5	10 s	

Table 2. Parameters of the Mie computations (Eq. 2) according to different particle populations. No value is given to the aerosol-droplet transition diameter as it is highly variable from a size distribution to another. Mean value was 4.0 ± 1.1 µm.

Contributing particles to extinction	D_{min} (µm)	D_{max} (µm)	Refractive index	Instruments
Most hydrated aerosols of the accumulation mode	0.8	2.5	$1.45 - 0.05i$	WELAS
Largest hydrated aerosols of the accumulation mode	2.5	Aerosol-droplet transition diameter	$1.33 - 0i$	WELAS
All particles contributing to extinction in fog	0.8	50	$1.45 - 0.05i$ / $1.33 - 0i$	WELAS+FM100 (junction diameter of 7 µm)

Enhanced extinction of visible radiation due to hydrated aerosols in mist and fog

T. Elias et al.

Table 3. Particle properties observed during the developed fog events of November 2011 at SIRTA. Fog and mist-fog-mist cycles are numbered as $f\#$ and XXX $c\#$, respectively, with XXX for the formation type (RAD = radiative cooling, STL = stratus lowering). ADV for advective was added to two events. The start time of the fog, and the duration of both fog and pre-fog mist events are given. Mean fog visibility (by DF20+) and LWC (by FM100) are also given, as well as the mean hydrated aerosol number concentration (by WELAS) and number concentration of all aerosol sizes (by CPC). Values are given as average ± SD, for each fog. The four last lines provide monthly averages, for all fogs, all pre-fog mists, all clear-air events (visibility > 10 km). The visibility value between parentheses in the "all fog events" row stands for the computed "droplets only" (Sect. 3.2).

Fog formation type and mist-fog-mist cycle number	Pre-fog mist duration (h)	Fog number	Fog start in Nov 2011	Fog duration (h)	Visibility (m)	Month average ± SD in fog LWC (mg m^{-3})	N_{ha} (cm^{-3})	N_C (cm^{-3}), with ambient size < 2.5 µm
RAD c1	/	f1	02, 00:45	7.25	140 ± 30	87 ± 41	210 ± 60	3300 ± 900
RAD c2	1.0	f2	10, 18:00	18.0	240 ± 130	50 ± 17	700 ± 410	3600 ± 1400
		f3	11, 12:30	5.0	600 ± 170	12 ± 4	390 ± 60	4400 ± 600
STL c3	4.75	f4	12, 03:00	4.25	380 ± 230	50 ± 26	620 ± 100	4200 ± 300
RAD c4	0.5	f5	15, 02:45	5.0	530 ± 190	18 ± 6	630 ± 100	7400 ± 4500
		f6	15, 08:45	1.0	760 ± 190	14 ± 6	460 ± 60	8100 ± 800
RAD c5	0.5	f7	16, 01:15	12.25	230 ± 140	63 ± 25	790 ± 450	5900 ± 2100
		f8	16, 15:15	8.75	230 ± 180	69 ± 29	900 ± 300	7300 ± 700
RAD c6	/	f9	23, 05:00	5.25	310 ± 230	83 ± 57	1040 ± 360	8800 ± 1300
STL c7	5.0	f10	24, 06:15	1.0	440 ± 260	37 ± 22	500 ± 40	5300 ± 800
		f11	24, 08:00	7.0	560 ± 290	32 ± 17	430 ± 60	4900 ± 700
		f12	24, 16:15	2.0	550 ± 190	30 ± 9	540 ± 50	3700 ± 500
STL c8	6.5	f13	25, 03:00	0.25	1630	11	/	1700
		f14	25, 03:30	0.75	920 ± 240	19 ± 1	/	1700 ± 400
STL c9	1.5	f15	25, 21:15	3.25	850 ± 340	23 ± 8	450 ± 50	2800 ± 300
		f16	26, 01:00	9.75	450 ± 500	77 ± 43	240 ± 90	3700 ± 1700
RAD/ADV c10	< 0.25	f17	28, 06:30	4.25	410 ± 240	53 ± 23	240 ± 100	7000 ± 2000
STL/ADV c11	< 0.25	f18	29, 08:30	1.0	1230 ± 390	15 ± 5	290 ± 30	6600 ± 1300
All fog events	19.75	/	96	380 ± 320	52 ± 35 (530 ± 490)	520 ± 320	5000 ± 2400	
All RAD/STL fog events	2/17.75	/	66.75/	290 ± 210/ 29.25	55 ± 35/ 570 ± 430	600 ± 350/ 48 ± 36	6400 ± 2600/ 360 ± 140	4000 ± 1400
All pre-fog mist events			/	/	3220 ± 1130	< 1	330 ± 100	5200 ± 2100
All clear-air events			/	/	21 000 ± 10 800	< 1	35 ± 30	9200 ± 5400

Enhanced extinction of visible radiation due to hydrated aerosols in mist and fog

T. Elias et al.

Title Page

Abstract | Introduction

Conclusions | References

Tables | Figures

|◄ | ►|

◄ | ►

Back | Close

Full Screen / Esc

Printer-friendly Version

Interactive Discussion

Table 4. Values of the average ratio $\mathrm{pec}_M/\mathrm{pec}_K$ for different events.

Event	Further conditions		$\mathrm{pec}_M/\mathrm{pec}_K$ (%)
	/		66 ± 32
	Cloud-free sky	/	78 ± 30
No-fog mist	Cloud-free sky	$\Delta T > 0.04°\,\mathrm{m}^{-1}$	53 ± 23
	Cloud-free sky	$\Delta T < 0.04°\,\mathrm{m}^{-1}$	95 ± 21
	Cbh < 100 m	/	43 ± 20
Pre-fog mist	/		86 ± 22
Fog	/		107 ± 35
Rain events ($\Delta T > 0.4\,\mathrm{mm\,h}^{-1}$)	/		25 ± 12

Table 5. Values of the aerosol extinction cross section (10^{-8} cm^2) computed by two methods, for different size intervals, for pre-fog mist and fog. The method "DF20+ and WELAS" means the slope is computed between pec_K and N_{ha}. The method "WELAS and Mie theory" means that pec_M is divided by N_{ha}.

Method	DF20+ and WELAS	WELAS and Mie theory		
Diameter range (µm)	Full range	$D < 2.5$	$D > 2.5$	Full range
Pre-fog mist	3.0	2.4 ± 0.4	/	2.5 ± 0.5
Fog	/	3.5 ± 0.5	15.8 ± 5.3	4.3 ± 1.1
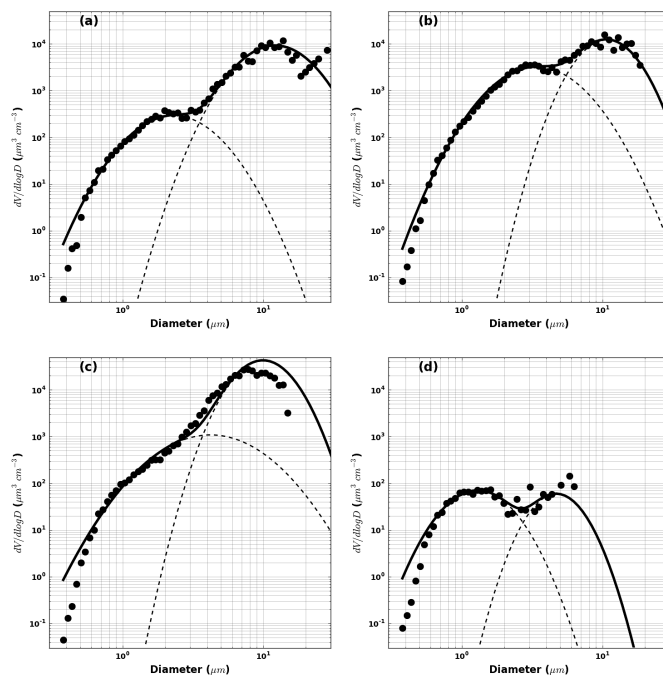
Figure 1. The particle volume size distributions measured by WELAS during 4 fogs of November 2011. Measurements are shown by dots, and approximations by log-normal distributions are shown by the lines, dashed lines for the monomodal distributions, and a thick continuous line for the bimodal distribution. **(a)** 2 November 02:00 UT, during fog f1, **(b)** 10 November, 20:00 UT, during fog f2; **(c)** 26 November, 06:00 UT, during fog f16; **(d)** 28 November, 07:30 UT, during fog f17.
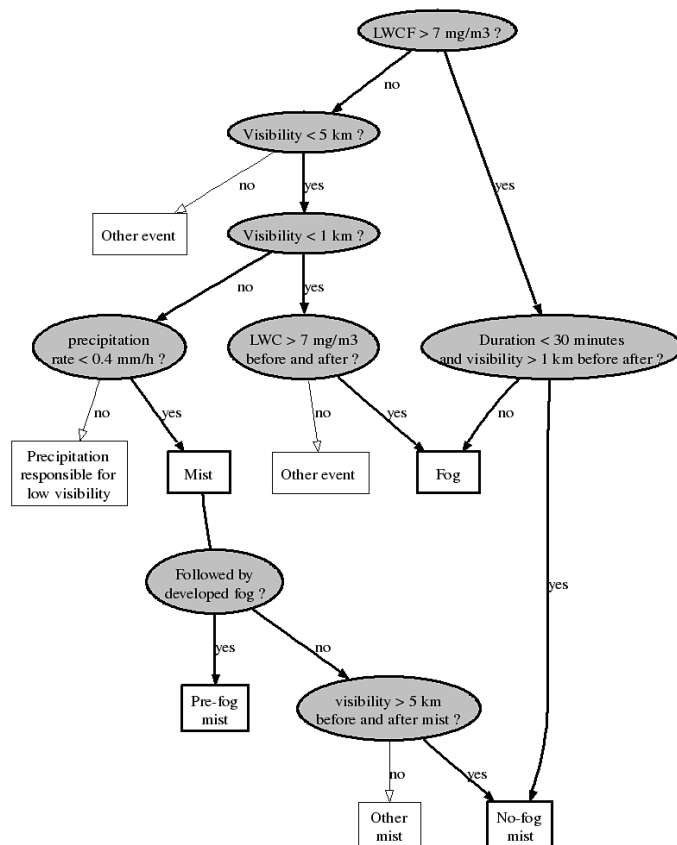
Figure 2. Flow chart of the pre-fog/no-fog mist and fog definitions, according to observations made at SIRTA in November 2011. DT stands for the thermal vertical gradient.
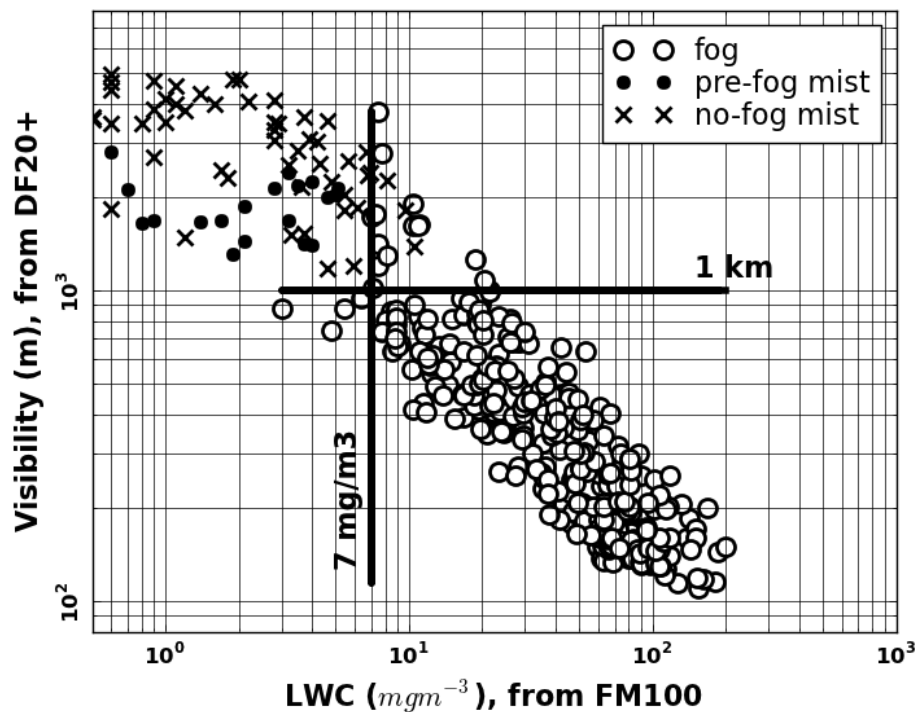
Figure 3. Relationship between visibility, observed by DF20+, and LWC, observed by FM100, during three regimes in November 2011 at SIRTA.

Title Page

Abstract | Introduction

Conclusions | References

Tables | Figures

|◄ | ►|

◄ | ►

Back | Close

Full Screen / Esc

Printer-friendly Version

Interactive Discussion
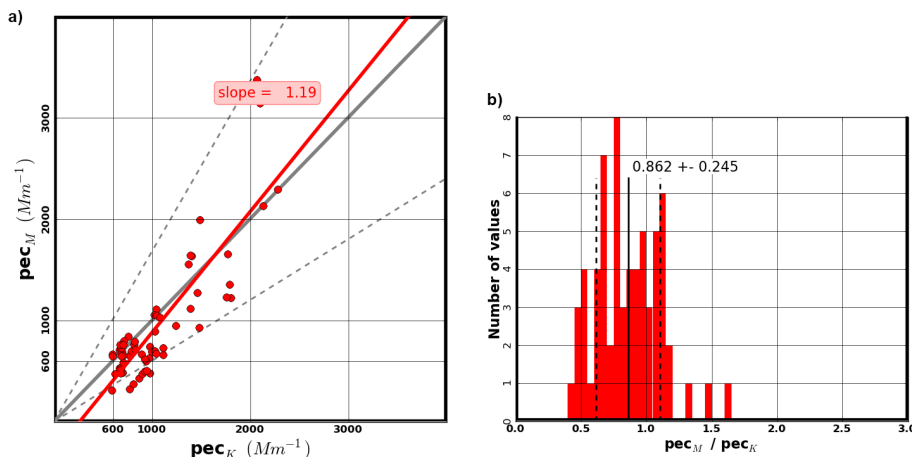
Figure 4. A comparison between the particle extinction coefficient measured by DF20+ (pec_K) and that computed by Mie theory (pec_M) applied on the size distributions measured by WELAS, in the pre-fog mist regime of November 2011. Refractive index is $1.45 - 0.05i$. **(a)** pec_M function of pec_K, the linear correlation is plotted in red, with corresponding slope value, and the 1 : 1 and the ±40 % lines are plotted in grey. **(b)** Frequency distribution of the ratio pec_K/pec_M. The average and standard deviation are written in black.

Title Page

Abstract | Introduction

Conclusions | References

Tables | Figures

|◄ | ►|

◄ | ►

Back | Close

Full Screen / Esc

Printer-friendly Version

Interactive Discussion
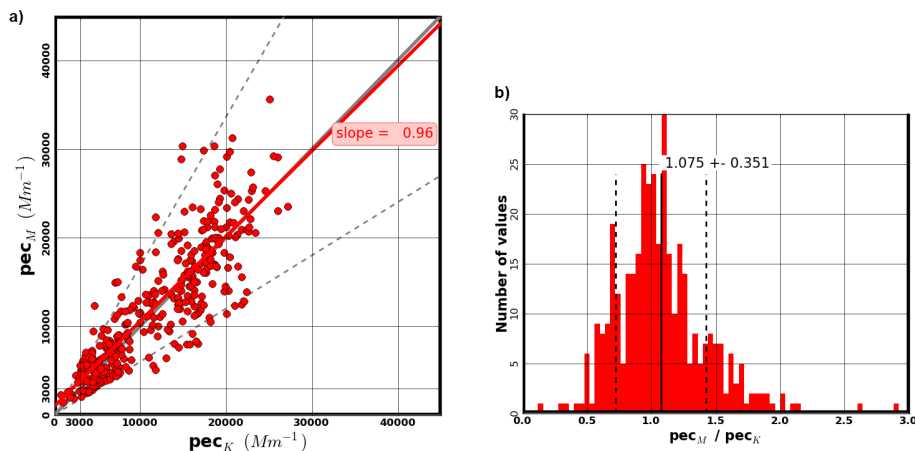
Figure 5. As in Fig. 4 but for the fog regime. The size distribution is generated by combining WELAS and FM100, and two values of the refractive index are used (see text).
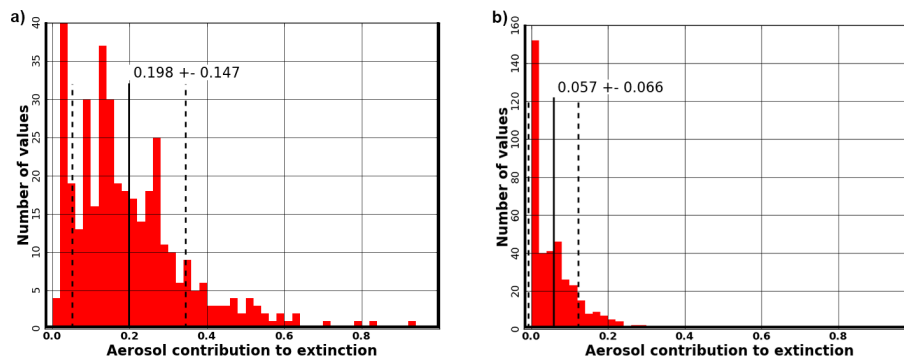
Figure 6. The contribution of hydrated aerosols to extinction of visible radiation in fogs observed during November 2011. **(a)** For aerosols smaller than 2.5 μm in diameter ($\Delta_{ha}pec_M$), **(b)** for aerosols larger than 2.5 μm ($\Delta_{D>2.5\,\mu m}pec_M$).

Title Page

Abstract | Introduction

Conclusions | References

Tables | Figures

|◄ | ►|

◄ | ►

Back | Close

Full Screen / Esc

Printer-friendly Version

Interactive Discussion
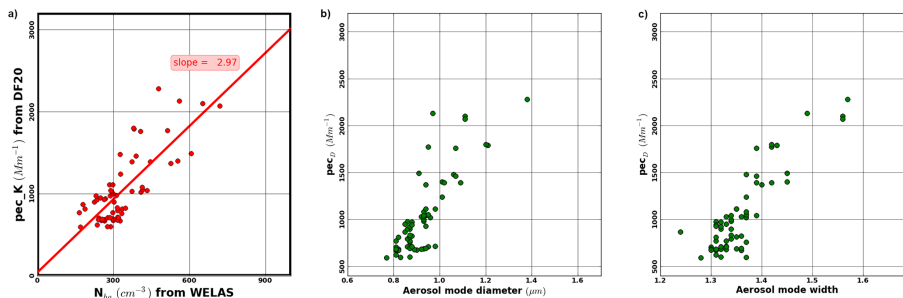
Figure 7. The relationship between the particle extinction coefficient (pec_K) directly measured by the DF20+, and the accumulation mode parameters: **(a)** aerosol mode number concentration (N_{ha}) (with the linear correlation in red), **(b)** mode diameter and **(c)** mode width.
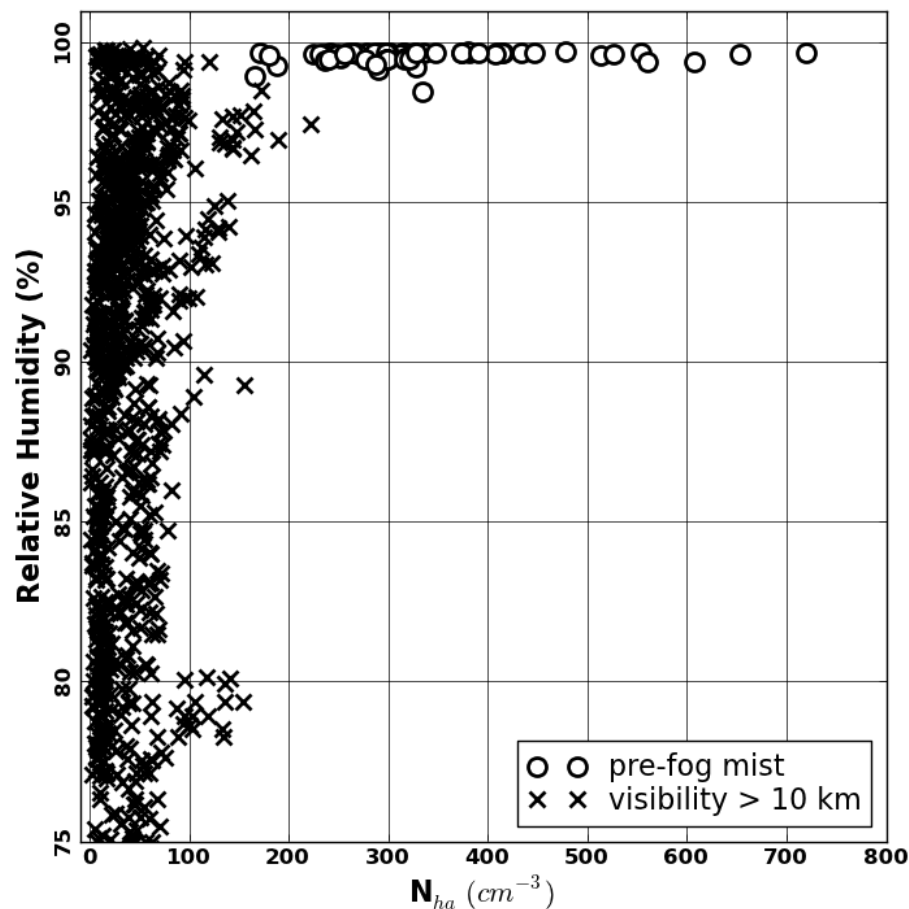
Figure 8. Correlation between relative humidity and the hydrated aerosol number concentration for two regimes: visibility > 10 km and pre-fog mist.

Title Page

Abstract | Introduction

Conclusions | References

Tables | Figures

|◀ | ▶|

◀ | ▶

Back | Close

Full Screen / Esc

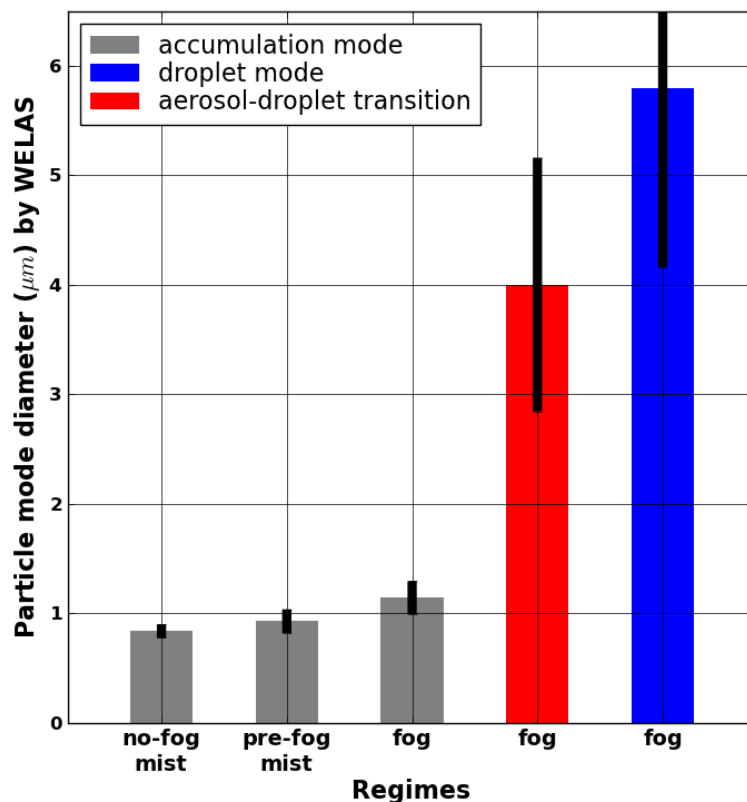Printer-friendly Version

Interactive Discussion

Figure 9. Monthly averages of the particle mode diameter derived from the WELAS data, for different regimes: accumulation mode in mist and in fog (grey), and droplet mode in fog (blue), as well as the aerosol-droplet transition diameter (red). Vertical thick lines depict the standard deviation.
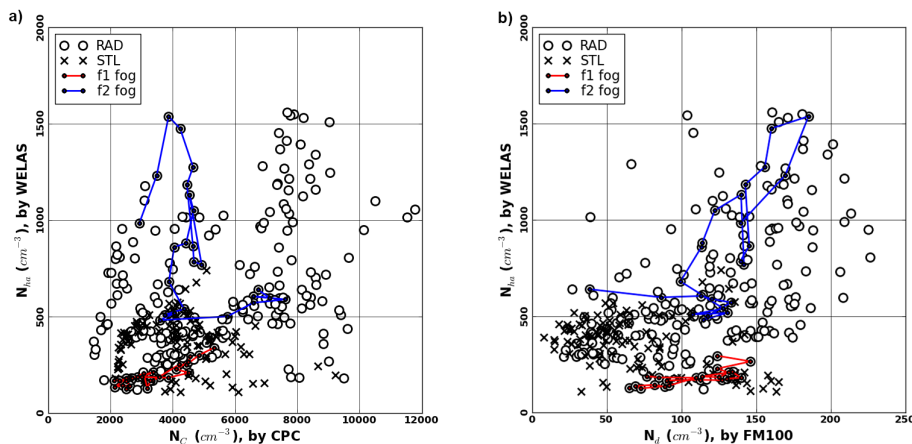
Figure 10. The relationships between number concentrations, marked according to the main formation process: left, the hydrated aerosol number concentration (N_{ha}) in function of all aerosol number concentration (N_C); right, N_{ha} in function of the droplet number concentration (N_d). Two RAD fog events are highlighted in red and blue.

Title Page

Abstract   Introduction

Conclusions   References

Tables   Figures

|◄   ►|

◄   ►

Back   Close

Full Screen / Esc

Printer-friendly Version

Interactive Discussion